

Structure of the black hole's Cauchy horizon singularity

Lior M. Burko

Department of Physics, Technion—Israel Institute of Technology, 32000 Haifa, Israel.

(May 8, 2019)

We study the Cauchy horizon (CH) singularity of a spherical charged black hole perturbed nonlinearly by a self-gravitating massless scalar field. We show numerically that the singularity is weak both at the early and at the late sections of the CH, where the focusing of the area coordinate r is strong. In the early section the metric is almost Reissner-Nordström, and the fields behave according to perturbation analysis. We find exact analytical expressions for the gradients of r and of the scalar field, which are valid at both sections. We then verify these analytical results numerically.

PACS number(s): 04.70.Bw, 04.20.Dw, 04.25.Dm

One of the long-standing interesting predictions of General Relativity (GR) is the occurrence of spacetime singularities inside black holes (BHs). This issue is intriguing, because the laws of physics we currently understand (e.g. classical GR) are not valid at singularities, but some other, as yet unknown, laws take over from classical GR and control the structure of singularities. Thus, despite many efforts in the last few decades, the nature of the spacetime singularities in a generic gravitational collapse—and, more generally, the final outcome of the collapse—are still open questions.

Until recently, the only known generic singularity was the BKL singularity [1]—an oscillatory spacelike singularity. In the last few years, however, evidence has been steadily accumulating that another type of singularity forms at the Cauchy horizon (CH) of spinning or charged BHs. The features of this new singularity differ drastically from those of the previously-known singularities like, e.g., Schwarzschild or BKL: First, the CH singularity is null rather than spacelike [2–4]; Second, it is weak [3,4]. Namely, the tidal distortion experienced by an infalling extended test body is finite (and, moreover, is typically negligibly small) as it hits the singularity [6]. Yet, curvature scalars diverge there [2,4] (in the spherical charged case, this is expressed by mass inflation [2]).

For uncharged spinning BHs (the more realistic case), the evidence in favor of this new picture emerges primarily from a systematic linear and non-linear perturbative analysis [4,5]. In addition, the local existence and genericity of a null weak singularity in solutions of the vacuum Einstein equations was demonstrated in Ref. [7]. (The compliance of null weak singularities with the constraint equations was demonstrated in [8].) In the case of a spherical charged BH, the weakness of the singularity was first demonstrated in [3]. More recently, an approximate leading-order analysis [9] confirmed the local consistency of this new picture.

Despite these recent advances, our understanding of the null weak CH singularity is still far from being complete. In particular, it is important to verify this new picture by performing independent, non-perturbative, anal-

yses. This motivates one to employ numerical tools to study the structure of the CH singularity. The numerical simulation of spinning BHs is difficult, as they are non-spherical. One is thus led to study, numerically, the inner structure of a spherical charged BH; hopefully, it may serve as a useful toy model for a spinning BH.

The first numerical analysis of a perturbed charged BH's interior was carried out by Gnedin and Gnedin [10], who analyzed the spherically-symmetric gravitational collapse of a self-gravitating scalar field over a charged background. The coordinates (and numerical grid) used there, however, do not allow getting even close to the CH. More recently, Brady and Smith (BS) [11] numerically explored the mass-inflation singularity inside a spherical charged BH perturbed nonlinearly by a scalar field. This analysis confirmed several aspects of the above new picture: It demonstrated the existence of a null singularity at the CH, where the mass function m diverges but the radial Schwarzschild coordinate r is nonzero. The quantity r was found to decrease monotonically with increasing retarded time along the CH, due to the nonlinear focusing, until it shrinks to zero (at which point the singularity becomes spacelike). It also provided evidence for the weakness of the singularity. Despite its remarkable achievements, however, this analysis left one important issue unresolved: To what extent is the perturbative approach applicable at (and near) the CH singularity? BS reported on an inconsistency with the predictions of perturbation analysis, manifested by the non-zero value of σ (see [11]), namely a finite deviation of the power-law indices from the integer values predicted by perturbative analyses. This issue is crucial, because for realistic (i.e., spinning and uncharged) black holes the only direct evidence at present for the actual occurrence of a null weak singularity stems from the perturbative analysis [4]. A failure of the perturbative approach in the spherical charged case would therefore cast doubts on our understanding of realistic black holes' interiors.

In this paper we report on a numerical and analytical investigation, which we carried out in order to answer this and other questions. We consider the model of a

spherical charged black hole non-linearly perturbed by a spherically-symmetric, self-gravitating, neutral, massless scalar field Φ (the same model as in [10,11]). We shall first present our numerical results which show that the CH singularity is indeed weak—not only in the early part of the CH, but also all the way down to the point of complete focusing ($r = 0$). Then, we study the asymptotic behavior of perturbations at the early part of the CH, and demonstrate the full compliance with the predictions of perturbation theory (in particular, we find that $\sigma \equiv 0$). In addition, we shall show that despite the divergence of m , the metric functions at the asymptotically-early part of the CH are remarkably close to the unperturbed Reissner-Nordström (RN) metric functions—which is again a prediction of the perturbation analysis (according to the latter, the metric perturbations should vanish at the asymptotic past “edge” of the CH, despite the divergence of the curvature [4]). Then, we shall analyze the behavior of the blue-shift factors $r_{,v}$ and $\Phi_{,v}$, as a function of u , at the late (i.e. strong-focusing) part of the CH, where u and v are ingoing and outgoing null coordinates, respectively (see below). The asymptotic behavior of $r_{,v}$ and $\Phi_{,v}$ is essential, because it is primarily these entities that are responsible to the divergence of curvature at the CH. We shall present exact analytic expressions for these entities, and verify them numerically. The expression we obtain for $\Phi_{,v}$, in addition to our numerical results, shows that σ vanishes not only at the early part of the CH, but also everywhere along it.

We write the general spherically-symmetric line element in double-null coordinates,

$$ds^2 = -f(u, v) du dv + r^2(u, v) d\Omega^2, \quad (1)$$

where $d\Omega^2$ is the unit two-sphere. As the source term for the Einstein equations we take the contributions of both the scalar field and the (sourceless) spherically-symmetric electric field (see [12] for more details). The dynamical field equations are

$$\Phi_{,uv} + (r_{,u}\Phi_{,v} + r_{,v}\Phi_{,u})/r = 0 \quad (2)$$

$$\begin{aligned} f_{,uv} &= \frac{f_{,u}f_{,v}}{f} + f \left\{ \frac{1}{2r^2} \left[4r_{,u}r_{,v} + f \left(1 - 2\frac{Q^2}{r^2} \right) \right] \right. \\ &\quad \left. - 2\Phi_{,u}\Phi_{,v} \right\} \end{aligned} \quad (3)$$

$$r_{,uv} = -\frac{r_{,u}r_{,v}}{r} - \frac{f}{4r} \left(1 - \frac{Q^2}{r^2} \right), \quad (4)$$

where the constant Q is the electric charge. Equations (2)–(4) are supplemented by two constraint equations:

$$r_{,uu} - (\ln f)_{,u}r_{,u} + r(\Phi_{,u})^2 = 0 \quad (5)$$

$$r_{,vv} - (\ln f)_{,v}r_{,v} + r(\Phi_{,v})^2 = 0. \quad (6)$$

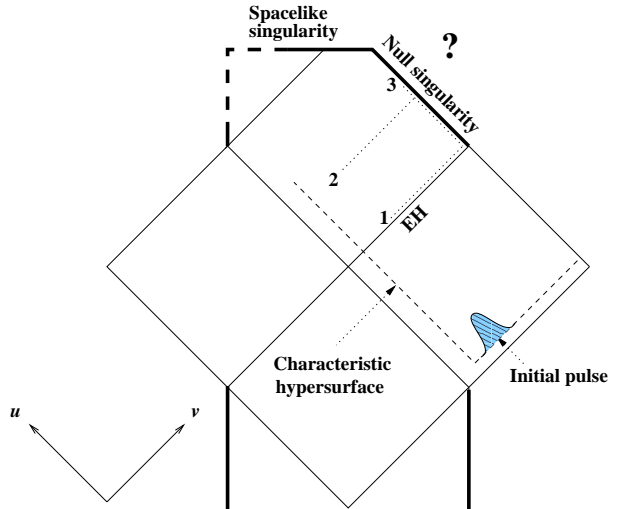


FIG. 1. The Penrose diagram of the simulated spacetime. Singularities are displayed by thick lines, and the characteristic hypersurface on which the initial data are specified are marked with dashed lines. The various fields are probed along outgoing (such as 1—in the early sections—and 2—in the late sections) and ingoing (such as 3) null rays. It is still unknown whether there is a continuation of the spacetime manifold beyond the CH. Our domain of integration cannot include the entire spacelike portion of the singularity. These uncovered areas are marked by dashed thick lines.

It turns out that it is advantageous to substitute $f(u, v) = 2e^{2s(u, v)}$ for the numerical integration near the CH. Our initial-value setup is described in Ref. [12]: The geometry is initially RN, with initial mass $M_0 = 1$ and charge Q , and no scalar field. At some moment v , however, it is modified by an ingoing scalar-field pulse of a squared-sine shape with amplitude A . Φ vanishes everywhere on the initial surface except in a finite range $v_1 < v < v_2$. The results presented below relate to $v_1 = 10$, $v_2 = 20$, $Q = 0.95$ and $A = 8 \times 10^{-2}$, unless stated otherwise. In this case, due to the scalar-field energy, the BH’s external mass approaches the final mass $M_f \approx 1.4$. (We also checked other values of $0.5 < Q/M_f < .99$ and A , and obtained similar results.) Note that our outgoing initial null hypersurface is located outside the event horizon (EH) (unlike in Ref. [11]). Therefore, we do not have to make any assumption about the inverse power tails at the EH; these are created automatically by the dynamical evolution. Our numerical scheme is essentially the same as described in Ref. [12] (there are few modifications, which will be described elsewhere [14]): It is based on free evolution in double-null coordinates. The code is stable and second-order accurate [12]. Our numerical setup is displayed in Figure 1, imbedded in the Penrose diagram of the simulated spacetime.

The null coordinates u and v are defined in Ref. [12]: They are taken to be linear with r on the two characteristic initial segments. For the presentation and interpre-

tation of the results, we shall occasionally use other types of double-null coordinates: Eddington-like coordinates u_e and v_e , and Kruskal-like coordinates (of the *inner* horizon of RN) U and V . (In the perturbed spacetime, the Eddington-like and Kruskal-like coordinates are defined with respect to the asymptotic “vertex” region, where the metric perturbations vanish asymptotically; see [14].) Recall that at $v \gg M_f$, v is closely related to v_e [12].

Our numerical simulations confirm the presence of a null singularity at the CH, where m diverges and r is nonzero. Along the CH singularity, r decreases monotonically, until it shrinks to zero, at which point the singularity becomes spacelike. This situation was already found numerically by BS [11].

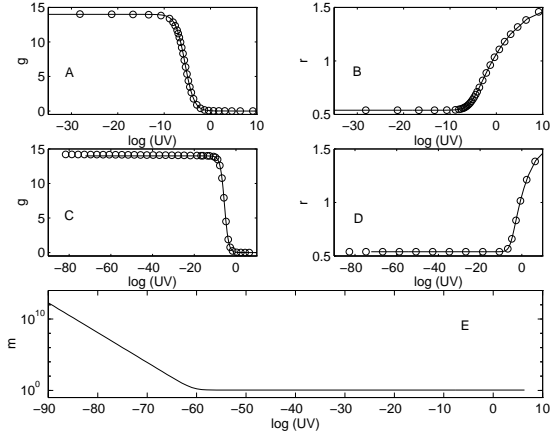


FIG. 2. Metric functions in the early sections of the CH. g [(A) and (B)] and r [(C) and (D)] as functions of $\log(UV)$ along an outgoing ray and an ingoing ray at $v = 80$, respectively. The solid lines are the RN values (computed according to the BH’s external parameters at $v = 75$), and the circles represent the numerical values. (E): The mass function along the same outgoing ray as (A) and (C). Here we took $N = 80$ and $A = 5 \times 10^{-2}$, which corresponds to $M_f \approx 1.1$.

We shall first discuss the early part of the CH singularity, i.e., the part where the focusing of r is still negligible. Our first goal is to demonstrate that the singularity is weak. In terms of the double-null metric (1), the singularity will be weak if coordinates $\hat{u}(u), \hat{v}(v)$ can be chosen such that both r and $g_{\hat{u}\hat{v}}$ are finite and nonzero at the CH. The numerical analysis by BS already demonstrated the finiteness of r , which we recover in our results. (Note that r is independent of the choice of the null coordinates.) Figure 2(A) displays the metric function $g \equiv -2g_{\hat{u}\hat{v}}$ in Kruskal-like coordinates U, V along an outgoing null ray that intersects the early section of the CH singularity. The CH is located at $V = 0$ (corresponding to $v \rightarrow \infty$). This figure clearly demonstrates the finiteness of g_{UV} , from which the weakness of the singularity follows.

The perturbation analysis also predicts that both the scalar field and the metric perturbations will be arbitrary-

ily small at the early section of the CH. In other words, both metric functions r and g should be arbitrarily close to the corresponding RN metric functions. This behavior is indeed demonstrated in Fig. 1. In this figure, g and r are displayed along lines $u = \text{const}$ [Figs. 2(A) and 2(B)] and $v = \text{const}$ [Figs. 2(C) and 2(D)]. The similarity of the analytic RN functions and the numerically-obtained functions of the perturbed spacetime is remarkable. (We emphasize, though, that despite the similarity in the values of the metric functions to RN, our geometry is drastically different from that of RN, in the sense that in our case curvature blows up at the CH.)

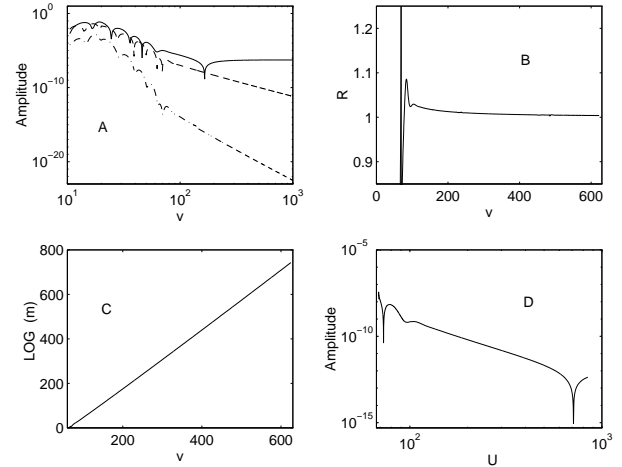


FIG. 3. Fields in the early sections of the CH. (A): Ψ (solid), $\Psi_{,v}$ (dashed), and $r_{,v}$ (dash-dotted) along an outgoing ray, as a function of v . (B): R , and (C): $\log m$, along the same outgoing ray, as a function of v . (D): Ψ along an ingoing ray, as a function of U .

The validity of the perturbation analysis is checked in more detail in Fig. 3, which displays the power-law behavior of $\Psi \equiv r\Phi$, $\Psi_{,v}$, and $r_{,v}$ near the early section of the CH. Fig. 3(A) displays these entities along an outgoing ray. Both the ringing and the power-law tails are apparent (the graph of Ψ approaches a nonzero limiting value, due to the finite value of U on that ray). Fig. 3(B) displays $R \equiv \Psi_{,v}/\Psi_{,v}^{\text{lin}}$, where $\Psi_{,v}^{\text{lin}} = \Psi_{,v}^{\text{EH}}[2(M_f/Q)^2 - 1]$ is the asymptotic form of $\Psi_{,v}$ as predicted by linear perturbation theory [13], and $\Psi_{,v}^{\text{EH}}$ is the (v -dependent) value of $\Psi_{,v}$ at the EH. Numerically, we find that at large v , R tends asymptotically to 1—it deviates from unity by no more than 2×10^{-3} at $v = 600$. A similar result was obtained for various values of Q and A . We thus find no evidence for charge-dependent internal power-law indices, and we conclude that the parameter σ of Ref. [11] vanishes identically. The behavior of m along the same outgoing ray is shown in Fig. 3(C). Clearly, the exponential growth of m does not affect the validity of the perturbation analysis. Finally, Fig. 3(D) displays Ψ along

an *ingoing* null ray at very large v . The local power index (see [12]) of u_e is found numerically to be 3.1, in a remarkable agreement with the value 3 predicted by linear perturbation theory. We conclude that the linear perturbation analysis describes the evolution of perturbation near the vertex well, despite the divergence of m (and the curvature). This confirms the prediction of nonlinear perturbation analysis [4], namely that nonlinear perturbations will be negligible at the early part of the CH, compared to the linear perturbations.

We turn now to explore the late part of the CH singularity, where focusing is strong. First, we numerically verify the weakness of the singularity in this part too. Figure 4(A) shows $G \equiv -2g_{uV}$ along an outgoing null ray in the late part of the CH, where the value of r has shrunk to 10% of the value it had when the CH was first formed. We present here the results for various values of the grid-parameter N (see [12]), in order to demonstrate the second-order numerical convergence. g_{uV} approaches a finite value at the CH ($v \rightarrow \infty$). At the same time, the mass function (and curvature) grows exponentially with v [see Fig. 4(B)]. We conclude that the entire null CH singularity is weak, even at the region of strong focusing.

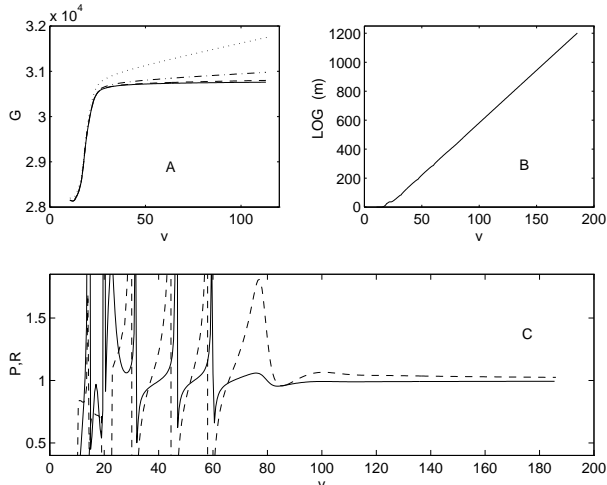


FIG. 4. The nonlinear regime (contraction of the CH of 90%): (A) G along an outgoing null ray, as a function of v . Dotted: $N = 20$, dash-dotted: $N = 40$, dashed: $N = 80$, and solid line: $N = 160$. (B) $\log m$ along the same outgoing ray. (C): R (dotted) and P (solid) along the same outgoing null ray, as a function of v .

Next we study, analytically, the behavior of the blue-shift factors $r_{,v}$ and $\Phi_{,v}$ along the contracting CH. Here, we shall present the results; the full derivation will be presented in Ref. [14]. The field equations (2) and (4) can be integrated exactly along the CH singularity [14]. For $r_{,v}$ we find

$$(r^2)_{,v_e} = -(1/\kappa_-) \Psi_{,v_e}^2, \quad (7)$$

and for $\Psi_{,v}$ we find

$$\Psi_{,v} = [2(M_f/Q) - 1] \Psi_{,v}^{\text{EH}}. \quad (8)$$

Here, κ_- is the surface gravity at the RN inner horizon with parameters M_f and Q . For convenience, Eqs. (7) and (8) are expressed in terms of Ψ . Note that (8) is invariant to a gauge transformation $v \rightarrow \tilde{v}(v)$, whereas (7) is not. [Eq. (7) refers explicitly to the derivatives with respect to the Eddington-like coordinate v_e .]

In order to verify this prediction, we calculated numerically $R \equiv \Psi_{,v}/\{\Psi_{,v}^{\text{EH}}[2(M_f/Q)^2 - 1]\}$ and $P \equiv -(r^2)_{,v_e}/[(1/\kappa_-)\Psi_{,v_e}^2]$, as functions of v , along an outgoing ray located at a region of 90% focusing of the CH. The results, presented in Fig. 4(C), are in excellent agreement with the above theoretical prediction, $R = 1 = P$.

To summarize, we have confirmed, numerically (for a spherical charged black hole) the main predictions of the perturbation analysis (which apply both to spherical charged and nonspherical, spinning BHs): The null singularity at the CH is found to be weak. In the asymptotic early section of the CH the metric functions approach arbitrarily close to the corresponding metric functions in RN, and, moreover, the perturbations are well described by the *linear* perturbation analysis. This confirms the conclusions of the perturbation analysis [4], that the nonlinear effects are negligible at the early section of the CH singularity. In addition, we analytically derived exact expressions for the diverging blue-shift factors $r_{,v}$ and $\Phi_{,v}$, which are valid everywhere along the contracting CH.

I am indebted to Amos Ori for numerous invaluable discussions and useful comments.

- [1] V. A. Belinsky, I. M. Khalatnikov and E. M. Lifshitz, *Advances in Physics* **19**, 525 (1970).
- [2] E. Poisson and W. Israel, *Phys. Rev. D* **41**, 1796 (1990).
- [3] A. Ori, *Phys. Rev. Lett.* **67**, 789 (1991).
- [4] A. Ori, *Phys. Rev. Lett.* **68**, 2117 (1992).
- [5] A. Ori, *Gen. Rel. Gravitation* (in press).
- [6] F. J. Tipler, *Phys. Lett. A* **64**, 8 (1977).
- [7] A. Ori and É. É. Flanagan, *Phys. Rev. D* **53**, R1754 (1996).
- [8] P. R. Brady and C. M. Chambers, *Phys. Rev. D* **51**, 4177 (1995).
- [9] A. Bonanno, S. Droz, W. Israel and S. M. Morsink, *Proc. R. Soc. London* **A450**, 553 (1995).
- [10] M. L. Gnedin and N. Y. Gnedin, *Class. Quant. Grav.* **10**, 1083 (1993).
- [11] P. R. Brady and J. D. Smith, *Phys. Rev. Lett.* **75**, 1256 (1995).
- [12] L. M. Burko and A. Ori, *Phys. Rev. D* (to be published), and Report No. gr-qc/9703067 (unpublished).
- [13] Y. Gürsel, V. D. Sandberg, I. D. Novikov, and A. A. Starobinsky, *Phys. Rev. D* **19**, 413 (1979).
- [14] L. M. Burko and A. Ori, in preparation.